Wolfgang Jacoby
Peter L. Smilde

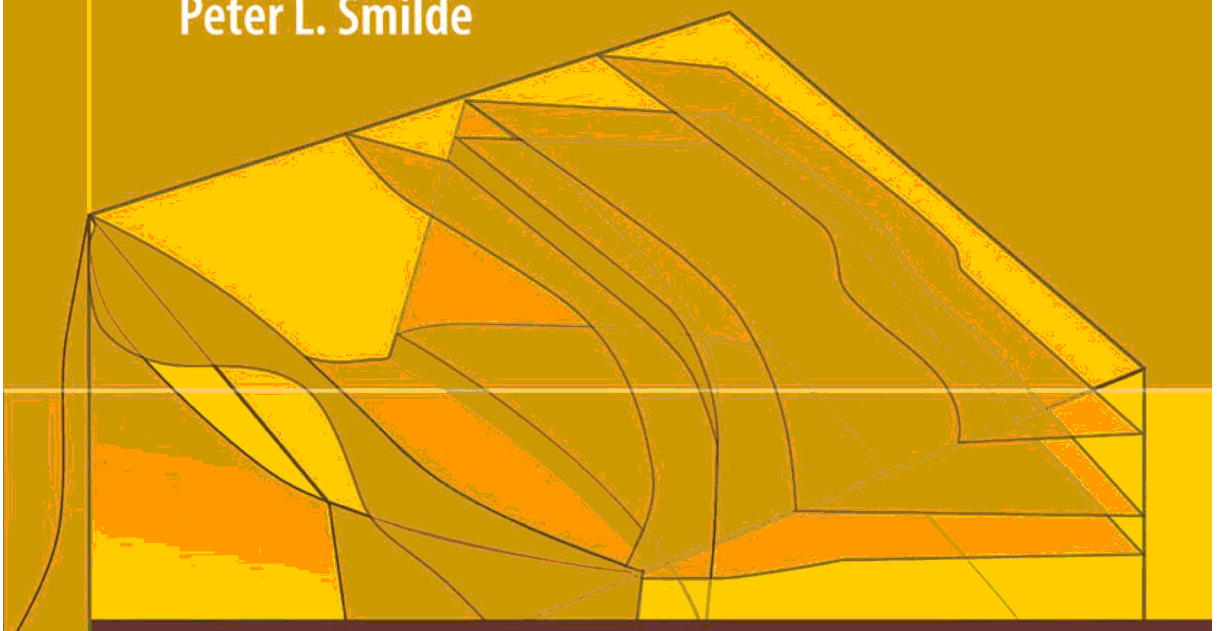

Gravity Interpretation

Fundamentals and Application of Gravity Inversion and Geological Interpretation

Springer

Preface vii
Many colleagues and friends in various institutions, not only from our own study field, have participated in teaching us this lesson, from our parents, families

viii Preface
and some school teachers to our academic teachers, Karl Jung†, Kiel, and Reiner Rummel, Delft, and to our later colleagues and students. Every one of them has chosen her/his own way and none is responsible for ours, but the – hopefully – mutual benefit has been immense. The intellectual challenges by colleagues and students are gratefully acknowledged. Geological teaching by Eugen Seybold, Kiel, and exchange with Richard Walcott, Richard Gibb, Alan Goodacre and Imre Nagy in Canada and with Gerhard M¨uller†, Frankfurt (Main), were important. In Mainz, Georg B¨uchel, Evariste Sebazungu, Tanya Fedorova, Ina Müller, Chris Moos, Michaela Bock, Herbert Wallner, **Hasan Çavşak**, Tanya Smaglichenko and many others **were influential on both of us.**
HerbertWallner helped intellectually by many discussions, with calculations and quite a number of figures. Tanya Fedorova provided some of the gravity inversion models. Evariste Sebazungu, in his own PhD thesis on potential field inversion, developed original ideas which entered into this treatise. **Hasan Çavşak** provided gravity calculations for various polyhedral bodies and helped discovering errors in some theoretical derivations. Pierre Keating provided information on some of the free modelling software. Discussions with Markus Krieger (Terrasys, Hamburg) led to several ideas and insights into the practical solution of interpretation problems. All of them and many more contributed thought-provoking ideas and thus influenced the present treatise. Most importantly, the mutual discussions between the authors through the whole time of their cooperation were beneficial to both. Finally, lecturing on gravity (and magnetics) taught us more than anything else to endeavour to present the ideas clearly.

Chapter 2
Fundamentals of Gravity, Elements of Potential Theory
SAHİFE 72-73

2.9.6.2 Massive Polyhedron
Massive polyhedra are flexible approximations to arbitrarily shaped geological bodies.
Their treatment somewhat differs from that of polyhedral shells (Sect. 2.9.5.2). The difference is in the infinitesimal mass elements. The size of the shell mass element ρ* d*s* depends on its orientation relative to the radius vector *r*, see (Eq. 2.9.12), and the arguments leading to it. In contrast, the mass element of the massive polyhedron is the oblique cone or pyramid expanded from ds and P (0, 0, 0); its volume is generally large relative to the infinitesimal dimensions of its base ds which, hence, is negligible and independent from the orientation of d*s*. Therefore the integration proceeds with mass elements ρd*V*, where d*V* is the volume of the infinitesimally thin cone defined by the solid angle dΩ whose volume grows with d*r* as d*V* = r^2 *r*d*r* dΩ; dΩ depends on the orientation as dΩ = cosψ d*s*/*r*2. If ds is at a given arbitrary r_0, *dV* = cosψ d*s*d*r*, and the volume of the cone Δ*V* depends on r

as cosψ $ds_0 \int^{r_0} dr$ = cosψ ds r_0.

The basic finite polyhedral elements Δ *s* are the variably oriented right triangles which, from P, expand massive oblique tetrahedra. For the plane-normal components, the planar elements are projected, as above, onto the unit sphere at P to directly render ΔΩ.

In the special case that the direction $\psi^{(E)}$ of the vector effect $\partial g^{(E)}$ is known, the components in *x*, *y*, *z* are found by back projection (Fig. 2.9.4): $\partial g_n{}^{(E)}$ = $\partial g^{(E)} cos\psi_n$, $\partial g_n{}^{(E)} cos\psi_h / cos\psi^E$. Generally, the vector or its direction is not known, and thus also the plane-parallel components must be calculated. The procedure is described by that for the polygon (Sects. 2.9.4.2 & 2.9.4.3; Figs. 2.9.7 & 2.9.8; Eqs. 2.9.29, 2.9.30, 2.9.31); integration of the massive oblique pyramid is reduced to $\int dh = h$ =, because the planar dh elements grow as h^2, compensating $1/r^2$. For each polyhedron triangle the vector is calculated in the local coordinates (*X*, *Y*, *Z*): $\delta g = \left(\delta_{gx}, \delta_{gy}, \delta_{gz}\right)$ and rotated into the global coordinates: $\delta_{gx}, \delta_{gy}, \delta_{gz}$ and added up component wise for the whole polyhedron, with *i* = 1, 2, 3 for *x*, *y*, z:

$$\delta g_i = \sum_{Sk} \delta g_{ik}$$

Another approach to calculating the gravity effect of a polyhedron(**Çavşak 1992**) is first to integrate the disturbing potential effect Δ*U* of an arbitrarily oriented pyramid from similar volume elements as used here and then calculating the vertical derivative $\delta g_z = \delta \Delta U / \delta z$ It requires coordinate transformations. The approach is facilitated by using vector calculus. Several solutions and algorithms of gravity integration over uniform polyhedra have been published, at least since the 1960s. Poh´anka (1988) and Holstein and co-workers in a series of papers (Holstein, 2002a,b; Holstein et al., 1999) summarized and compared them with each other, especially in view of computational precision. Polyhedra are treated with the aim to unify the calculations of what is called the “gravimagnetic effects” and to make optimal use of similarities common to all these related potential field problems. The methods may be distinguished as vertex, line and surface methods. The formulations are essentially all alike, but the approach is different: abstract, mathematical, based on the application of Gauss’ and Stokes’ integral theorems. In contrast, it is here attempted to design tailored mass elements (solid angle and vertical mass line, both growing with r^2) in a more visual approach. It encompasses special cases where mass elements degenerate to zero (on a polyhedron facet, an edge or a vertex)
where analytical treatment has problems. Computational aspects are discussed in Chap. 6.

Chapter 2
SAHİFE 84-85

2.9.8 Two-and-a-half Dimensional Models $\left(2\frac{1}{2}D\right)$

Two-dimensionality leads to significant errors of gravity calculation, if the length over depth ratio is not large. It is therefore advisable to estimate the errors. For this purpose, one can calculate the end corrections for finite length λ , i.e. by the factor a (Eq. 2.9.8) or construct simple 3D models for comparison.

It is tempting to save the simplicity of the 2D modelling by formulations generally applying end corrections of the 2D models and performing what has been called 21/2 dimensional modelling. However, while infinite length is never realistic, the limited lengths are usually difficult to define. The lateral extent of geological structures is often roughly known or can be inferred from the gravity maps, but it is generally uncertain what lies beyond the limited body and usually varies in three dimensions with significant gravity effects. In many cases it is best to immediately construct 3D models, but these aspects are the topic of Chap. 6.

Remark 2

Çavşak's (1992) integration of δg_z for *polyhedra* is based on the basic tetrahedra expanded from P to the arbitrarily oriented plane triangles (corners A, B, C, equivalent to vectors *A,B,C*) taken as the basic mass elements $\rho\Delta V$. First the potential δU of the mass element is calculated in a suitable Cartesian coordinate system (*X*, *Y*, *Z*) before $\delta g = \partial\delta U/\partial z$ is derived. *X* is chosen parallel to the side *AB*, *Z* parallel to *AB*×*BC* and *Y* normal to *X* and *Z*, i.e. parallel to the plane ABC. Integration is then fairly simple, being similar to the solid angle approach. To derive δg_z requires a rotational coordinate transformation (2.3.3.1) from (*X*, *Y*, *Z*) back to (*x*, *y*, *z*), for which we need the matrix of the components of the vector *x* = (*x,y, z*) or *xi*(*i* = 1,2,3) in the *X* = (*X,Y,Z*) or *X*k (k = 1, 2, 3) system; the matrix elements are cos(*xi,Xk*) of the angles between all *xi,Xk*. Since the *Xk* are defined in (*x*, *y*, *z*), their *x*, *y*, *z* components cos(*x*i,*X*k) = cos(*Xk,xi*) are known. Numerical routines for elementary vector and tensor (or matrix) operations facilitate the calculations. The potential and gravity effects $(\delta U, \delta g)$ of a polyhedron of triangles are derived by summing the contributions of all tetrahedra with a proper sign convention. Each edge separates two triangles and occurs thus twice. The final expression is principally the sum of functions of all corner points, i.e. their *x*, *y*, *z* coordinates, with the sign depending on the orientation of each triangle or the sign of the scalar product of *r.n*, where *n* is the outward surface normal vector. Details are in the dissertation by **Çavşak** (1992).

Chapter 2
SAHİFE 110

References

Çavşak, H.: Dichtemodel f¨ur den mitteleurop¨aischen Abschnitt der EGT aufgrund der gemeinsamen Inversion von Geoid, Schwere und refraktionsseismisch ermittelter Krustenstruktur. *Ph.D. thesis, Mainz*, 1992

Chapter 5
Qualitative Interpretation
SAHİFE 226-228

5.7.9 Mantle Convection

Mantle flow is largely hidden below the lithospheric plates which together are an integral convecting system. Effects in the gravity field are expected from related temperature and, hence, density variations. The relation between plates, deeper mantle flow and gravity is, however, not simple, as is evident in comparisons of the plate geometry and the global gravity field (see Sect. 1.5.4, 1.5.5; National Academy Press, 1997). Expansion in spherical harmonics of gravity and plate geometry suggests some correlation in harmonic degrees and orders 4 and 5 (Schubert et al., 2001), but the largest amplitudes are of degrees 2 and 3 which probably do not directly reflect plate-related flow. Low degree spherical harmonic components would certainly suggest mantle wide anomalies, but shallower anomalies of broad lateral extent are not excluded. Seismic tomography must be taken into account in view of velocitytemperature- density relations. A qualitatively important aspect is the Earth's tendency to orientate its axis of largest inertia parallel to its axis or rotation (Goldreich & Toomre, 1969) and this would tend to place the equator where convection upwellings predominate, thus hinting at a significant component of the flow pattern. Some component of gravity may, nevertheless, be more directly related to the moving plates, for example, through the continuity condition which requires the plate motion to be linked with flow. Respective data are difficult to isolate from the global gravity field which is an integral of all masses of Earth. Stacking gravity profiles along plate motion trajectories toward the trenches may enhance such a signal while suppressing other components. Examples are shown in Fig. 5.7.9a (after Seidler et al., 1983) where the *FA* is plotted along the trajectories of plate motion relative to the hotspot frame of reference versus distance (coordinate *X*B in degree) from the trailing edge (*X*B = 0) to the leading edge; the figure shows

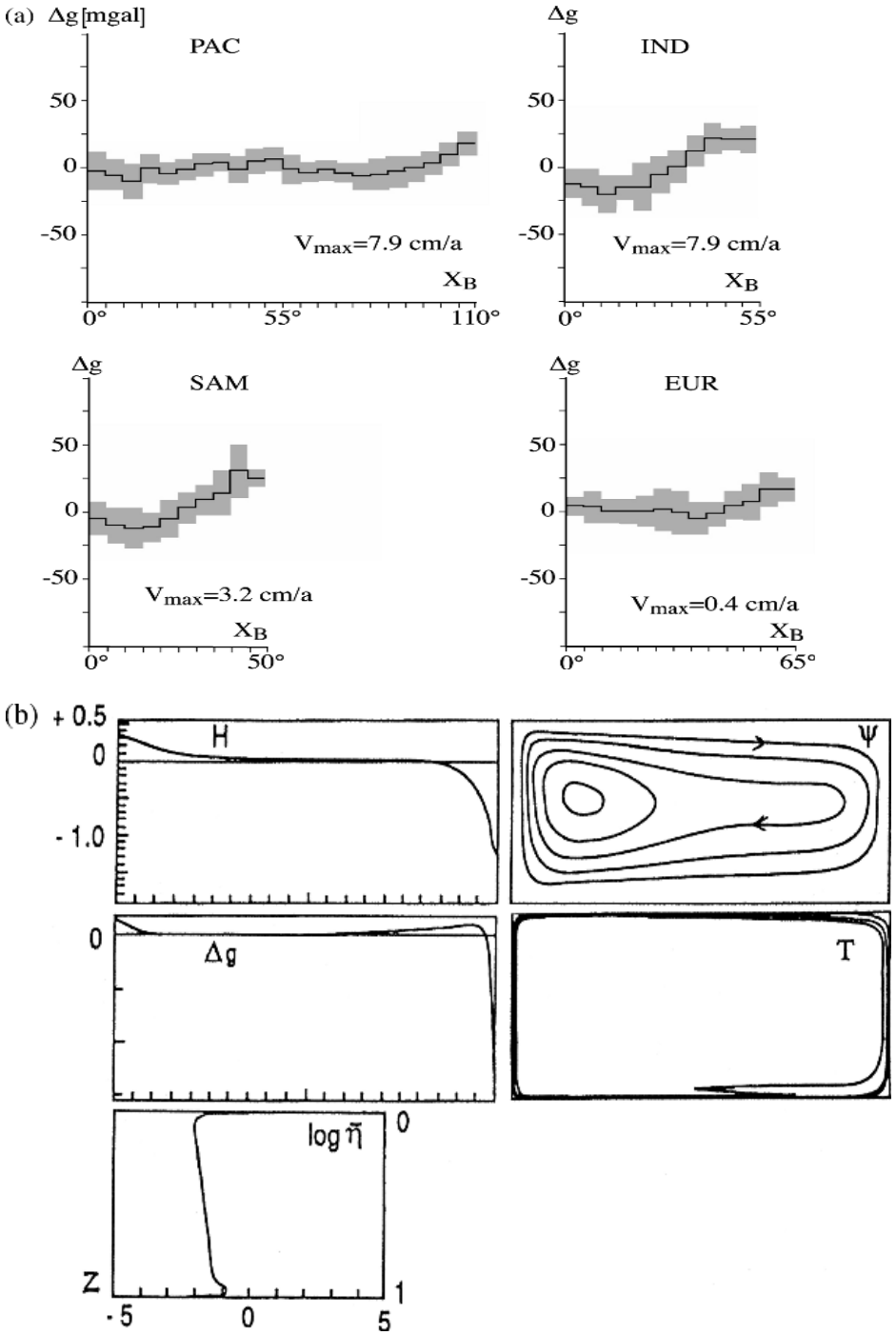

Fig. 5.7.9 Mantle convection. (**a**) FA plotted along trajectories of plate motion in hotspot frame of reference versus distance *X*B (in degree) from trailing edge (*X*B = 0) to the leading edge; *FA* averaged for *X*B = const (across the trajectories) shown as a bar, standard deviation shown in *grey*. Plates PAC, SAM, IND, EUR move from divergent to convergent boundaries. (**b**) Numerical model of convection in Cartesian box (Rayleigh number Ra = 106 with temperature dominated p, T-dependent viscosity (Ritzert & Jacoby, 1992); *boxes* show calculated elevation H (below water), *flow lines* as stream function contours Ψ; the *FA* gravity anomaly Δ *g*; the temperature field T; horizontally averaged viscosity as log η. (scales are dimensionless; note especially the relative variation of H and Δ *g*)

the averages for *X*B = const across the trajectories. The plates PAC, SAM, IND, EUR have in common the movement from divergent to convergent boundaries. They show a consistent trend of slight to distinct FA increase toward both ends, trailing

(divergent) and leading (convergent, i.e. subducting or overriding a subducting plate). Since the analysis smears out the effects, their amplitudes will appear subdued

and the widths enhanced (divergence: $\sim 10 \pm 10$mGal, $15^0 \pm 5^0$ width; convergence:

$20 \pm >10$mGal, $30^0 \pm 5^0$ width). Stacking of profiles across the spreading ridges in the Atlantic, Indic and Pacific render mean topographic highs of 1.0 to 1.6 km, mean *FA* highs of 6 to 14 mGal and mean *BA* lows of −80 to −130mGal, relative to the adjacent basins (Jacoby & **Çavşak**, 2005). Stacking and averaging does not fully suppress other independent effects; compare, for example, the plumeaffected Reykjanes Ridge (Sect. 5.7.6) with *FA* rising to +60mGal and *BA* only −60 to −80mGal. In the gravity disturbance (see Sect. 4.3) the positive effect is enhanced relative to the *FA* by the height reduction from the geoid to the ellipsoid ($N\partial g n/\partial h \times(-1) \approx +0.3086N$ [m]), as the geoid above upwelling flow (plume, ridge) is positively disturbed; this effect is somewhat lessened by the corresponding geoidal Bouguer reduction (see Sect. 4.5.3.1). In the *BA* the Bouguer reduction removes the effect of only the displaced surface not that of similarly displaced internal density contrast surfaces (e.g. Moho).

Chapter 5
SAHİFE 230

References

Jacoby, W.R., **Çavşak, H.**.: Inversion of gravity anomalies over spreading oceanic ridges. *J. Geodynamics*, 39, 461–474, 2005.

Chapter 6
Quantitative Interpretation
SAHİFE 244

6.2.1.2 Indirect Interpretation Methods with Few Large 2D Bodies

Indirect interpretation by trial and error model adjustment can be realized with any of the above parametrizations. The geometrical model description should be flexible without requiring a very large number of parameters. Rectangular cross sections may be useful in some cases. The classical method is based on the polygonal section or the “Talwani method”. It permits an efficient description, and change, of arbitrary shapes by relatively few parameters (corner coordinates). “Thin” horizontal layers, also vertical or oblique “dykes” and “thick” rectangular cross sections provide practical approximations to 2D bodies. The undulated density contrast surface is well suited for the trial and error approach.

(1) The expressions for numerical evaluation of the effects of 2D *oblique steps and polygons* (“Talwani method”) are Eqs. (2.9.61, 2.9.64 and 2.9.65). They contain angles and distances which generally must be calculated from coordinates (xi, zi) of observation points Pi(i = 1 to n) and (xk, zk) of corner points k (k = 1 to m; where the last point k =m is identical to the first point k =1). Tests should always be made

before “imported” routines are used for “production runs”.
A specific polygon is assigned its constant density contrast Δρ (Sect. 6.1.5.1 and Fig. 6.1.1). The corner points are read in sequence, usually clockwise along the polygon; programming then takes care of the calculated effects δ *g* to be positive if Δρ is positive and P essentially lies above the main part of the body. Changing the direction to anticlockwise, changes the sign of the effects. Complex models are built of several bodies which may be apart from each other, in contact or overlapping (see Fig. 6.1.1). Nesting or multiple wrapping (Fig. 6.1.1d) is an easy way to realize small stepwise or nearly continuous density variations, and an example is the calculation of the thermal expansivity, for example, of the cooling lithosphere at spreading ocean ridges **(Jacoby & Çavşak, 2005).**

Chapter 6
SAHİFE 249-250

6.3.1.2 Indirect Interpretation Methods with Few Large 3D Bodies
Indirect interpretation by trial and error cannot be standardized for the determination of depth, shape and density of 3D mass anomalies. The analytical expressions for the foreward calculations are presented in Sect. 2.9.6. For some purposes, graphical methods with templates were used before the advent of efficient computers (see Sect. 6.1.4). Methodological possibilities are briefly sketched here. The most flexible parametrizations, suitable for analytical and numerical evaluation and approximation of arbitrary shapes are probably the polyhedra (Sect. 2.9.6.2) and stacks of horizontal polygonal discs (Sect. 2.9.4.2) by which given contour lines can be exploited; for special cases, as “thin dykes” of laterally limited extent, equations for planar elements (Sects. 2.9.3.3 & 2.9.3.4) can be derived by coordinate rotation (Sect. 2.4.3.1). Cuboids and other regular (Sect. 2.9.6.1) bodies are less flexible to fit realistic 3D shapes. Cylinders or cones can be taken for crater-like bodies.

(1) *Massive polyhedra* (Sect. 2.9.6.2) with arbitrary complexity are generally applicable. One way is to first derive a set of vertical polygonal sections of anomalous masses from geology or geophysical models. Then triangulation can connect the sections. The gravity effects are finally calculated with expressions given by several authors (IGMAS: Götze & Lahmeyer, 1988**; Çavşak, 1992**; Holstein et al., 1999, Holstein, 2002a, b). Such methods permit a highly detailed description of 3D shapes, but they require large numbers of geometrical parameters (coordinates) and the sensitivity of the gravity effects to details and changes in detail may be low. Furthermore, detailed parametrization leads to the numerical evaluation of very many, very small contributions to the total gravity effect of a polyhedron, such that rounding errors may become a problem (see Holstein et al., 1999). Large numbers of parameters restrict the possibilities of formal inversion (Chap. 7).

Chapter 6
SAHİFE 263-264

6.5.6 Spreading Ridges
Before the advent of seafloor spreading, ocean ridges were considered submarine mountain belts with crustal roots, but then it was realized that hot, low-density material rises diapir-like and explains the ridge topography (Jacoby, 1970). In Sect. 5.7.6,

a qualitative estimate for Reykjanes Ridge of a density anomaly of –30kg/m3 for an assumed 100m depth extent was interpreted with a temperature anomaly of about +300K. Quantitative gravity modelling (2D: Sect. 6.2.1.2 (1)) has to take into account additional a priori information, mainly data on bathymetry and from seismic studies of crustal structure which shows the Moho to rise towards the ridge axes, instead of dipping with a thickening root. The Reykjanes Ridge was investigated by many workers (see Jacoby et al., 2007, and references quoted there). Here an interpretation of gravity across two ridges is reproduced: the rather slow Mid Atlantic Ridge (MAR: Fig. 6.5.6a), and the fast spreading East Pacific Rise (EPR: Fig. 6.5.6b). The 2D model of a triangular-shaped low-density body of hot rising asthenospheric mantle material from under the diverging cooling and thickening plates was adopted and adjusted by trial and error (Jacoby, 1978, where the available a priori information is quoted). Again, 2D is well justified, although the structures reach more than 50 km depth. Fitted was a modified *BA* reduced for crustal structure, i.e. crust was, so to speak, first “filled up” to mantle density by calculation (Sect. 4.5.3.1). The resulting gravity anomaly should essentially reflect the effect of the asthenospheric wedge.

The shape of the asthenosphere wedge is taken as an equivalent to the density distribution inherent in the isotherms of cooling plates, which should be quite similar in both ridges if normalized to a common spreading rate. It is the physically correct temperature model (McKenzie, 1977, but the asthenospheric wedges is a suitable equivalent. For the MAR with a wedge of 60 km height Δρ was found

Fig. 6.5.5 The SE Iceland shelf, compare Fig. 5.7.5. Four different model types portraying different geological processes which might have formed the shelf. (1) Non-isostatic edge fitted to the residual Bouguer anomaly, *rBA*; Moho and water body shown for comparison; (2) fit of *BA*: glacial abrasion causing uplift and enhanced average crustal density, coupled with sediments at the foot of the shelf slope; (3) fit of *rBA*: dense upper crust due to increased volcanism and forward building of shelf, coupled with light slope sediments; (4) fit of *rBA*: fully non-isostatic edge bending or rotation, uplifting the outer shelf and depressing the slope (see text)

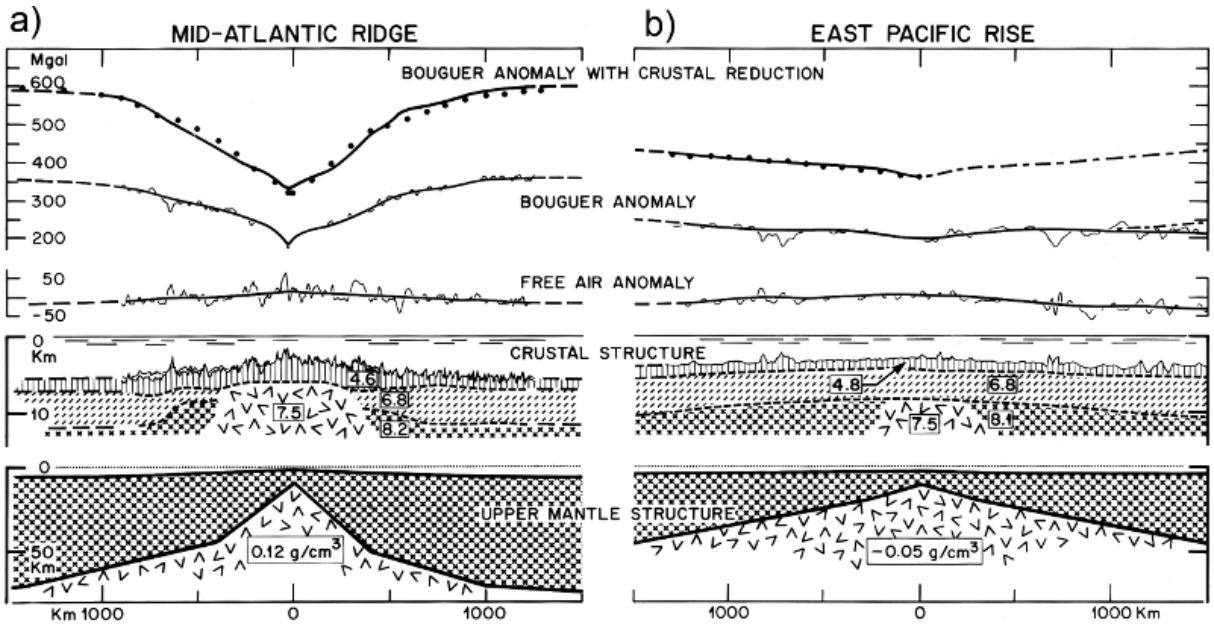

Fig. 6.5.6 Crust-upper mantle sections of spreading ridges, (**a**) Mid Atlantic Ridge (MAR), (**b**) East Pacific Rise (EPR); the sections are based on crustal seismic information (in boxes: seismic P velocities in km/s) and on the concept of thickening lithosphere and rising asthenosphere (after Jacoby, 1975)

to be about –120 kg/m3; this is a high value which, for a height of 100 km, would be reduced to about –70kg/m3, still exceeding estimates for the Reykjanes Ridge. For the EPR a much lower density contrast of –50kg/m3 for the central wedge with, however, only 30 km height was obtained (only –15kg/m3 if the height were 100 km).
The discrepancies between the preliminary estimate of Chap. 5 and the present models reflect the limitations of rough estimates, but the differences between the ridges seem substantial enough to be significant. The MAR and EPR are different, for example, in divergence rate, plume occurrence and dynamics. The slow spreading Atlantic is characterized by many near-ridge plumes that inject hot and possibly volatile-rich material into the asthenosphere, thus enhancing the melting and the density deficit, while the fast spreading Pacific is also driven by slab pull such that the asthenospheric upwelling might lag behind. The physically more adequate model of the lateral cooling density anomalies (anomalous isotherms; McKenzie, 1977) is treated by **Jacoby & Çavşak, (2005).**